Applied Physics Letters

RESEARCH ARTICLE | AUGUST 28 2023

# Mid-infrared Kerr index evaluation via cross-phase modulation with a near-infrared probe beam

D. Lorenc ; Z. Alpichshev

Check for updates

*Appl. Phys. Lett.* 123, 091104 (2023)
https://doi.org/10.1063/5.0161713

View Online
Export Citation
CrossMark

## Articles You May Be Interested In

Setting up Z-scan experiment to study nonlinear optical properties of polymer composites: Characterization of ADP doped PVA/PVP polymer films

*AIP Conference Proceedings* (April 2018)

Measurements of third-order optical nonlinearity using Z-scan technique: A review

*AIP Conference Proceedings* (August 2019)

Study of x-ray phase-shifting masks for sub-70 nm patterning

*Journal of Vacuum Science & Technology B: Microelectronics and Nanometer Structures Processing, Measurement, and Phenomena* (January 2001)

20 September 2023 11:35:16

500 kHz or 8.5 GHz?
And all the ranges in between.
Lock-in Amplifiers for your periodic signal measurements

Find out more
Zurich Instruments

AIP Publishing

Applied Physics Letters ARTICLE pubs.aip.org/aip/apl

# Mid-infrared Kerr index evaluation via cross-phase modulation with a near-infrared probe beam

Cite as: Appl. Phys. Lett. **123**, 091104 (2023); doi: 10.1063/5.0161713
Submitted: 11 June 2023 · Accepted: 10 August 2023 ·
Published Online: 28 August 2023

View Online Export Citation CrossMark

D. Lorenc[a] and Z. Alpichshev[b]

## AFFILIATIONS

Institute of Science and Technology Austria, Am Campus 1, 3400 Klosterneuburg, Austria

[a]Also at International Laser Center, Ilkovicova 3, 84104 Bratislava, Slovakia.
[b]**Author to whom correspondence should be addressed:** alpishev@ist.ac.at

## ABSTRACT

We propose a simple method to measure nonlinear Kerr refractive index in mid-infrared frequency range that avoids using sophisticated infrared detectors. Our approach is based on using a near-infrared probe beam which interacts with a mid-IR beam via wavelength-non-degenerate cross-phase modulation (XPM). By carefully measuring XPM-induced spectral modifications in the probe beam and comparing the experimental data with simulation results, we extract the value for the non-degenerate Kerr index. Finally, in order to obtain the value of degenerate mid-IR Kerr index, we use the well-established two-band formalism of Sheik-Bahae *et al.*, which is shown to become particularly simple in the limit of low frequencies. The proposed technique is complementary to the conventional techniques, such as z-scan, and has the advantage of not requiring any mid-infrared detectors.

*© 2023 Author(s). All article content, except where otherwise noted, is licensed under a Creative Commons Attribution (CC BY) license (http://creativecommons.org/licenses/by/4.0/).* https://doi.org/10.1063/5.0161713

20 September 2023 11:35:16

Nonlinear optical frequency conversion has gone a long way in the past decades from the initial observation of faint second-harmonic generation in the 1960s[1] to the present day when nonlinear-optics-based sources of coherent broadband radiation have become a staple of a modern optics lab.[2] Given the importance, there is a continual effort to improve the efficiency of such devices and, as one possible direction, it was demonstrated that many of the relevant nonlinear frequency-conversion phenomena—be it high-harmonic generation[3,4] or the production of strong THz-range pulses through optical rectification[5]—become particularly efficient when the frequencies of the primary (fundamental) pumping beams happen to lie in the mid-infrared domain. Naturally, the progress within this approach is contingent upon detailed characterization of the optical properties of nonlinear materials in the infrared range.

Kerr effect (KE) is a nonlinear optical phenomenon, wherein the refractive index of a material is changing as a response to the application of an external electric field. Unlike the closely related Pockels effect, KE is proportional to the square of the field and hence does not require broken inversion symmetry in the host medium.[6] In fact, it is virtually ubiquitous and manifests itself prominently in many different contexts, being responsible for a great number of phenomena, such as self- and cross-phase modulation of the beams, Kerr lensing, self-focusing, optical soliton formation, optical switching, passive mode-locking,[6] etc., and as such has to be taken into account when designing any practical nonlinear optical application.

The magnitude of KE is determined by the so-called nonlinear Kerr index $n_2$. On the conceptual level, the problem of measuring $n_2$ is long solved, thanks to advent of techniques such as z-scan,[7] I-scan,[8] four-wave mixing,[9,10] nearly degenerate three wave mixing,[11] two-beam coupling,[12] and a number of interferometric techniques (e.g., Ref. 13) However, in practice, it may still pose considerable challenges, especially when it comes to the mid- and deep-IR wavelengths where experiments require specialized components (most notably detectors) and often are not as straightforward as they are with visible or near-IR radiation. As a result, the amount of information on mid-IR Kerr refractive indices is comparatively scarce and even in the case of some standard materials, mid-IR Kerr index has been characterized only recently for a limited number of wavelength values.[13–15]

In this Letter, we propose to go around this issue by dropping the challenging part of mid-IR detection altogether and use a near-IR probe to gauge the changes to optical properties of a material as a response to mid-IR radiation. To this end, we study the non-degenerate Kerr effect-mediated interaction[16] between near- and mid-IR pulses manifested as cross-phase modulation (XPM)[6] between the two. Specifically, we observe the mid-IR pump-induced spectral changes in the probe pulse from which we extract the value for


© Author(s) 2023

non-degenerate Kerr index $n_2(\Omega, \omega)$. We, then, use the well-established two band theory of Sheik-Bahae *et al*[17] to reconstruct from $n_2(\Omega, \omega)$ the mid-IR Kerr index. The convenience of the proposed methods is especially apparent in the limit where both pump and probe photon energies are significantly less than the bandgap. In this regime, the two-band model predicts that relationship between the degenerate and non-degenerate Kerr indices becomes particularly simple and universal, the only material-specific property being the bandgap width that enters as a simple scaling factor for frequencies.

Thanks to its ubiquitous nature, Kerr effect can, in principle, be observed in any medium, provided it is transparent in the relevant wavelength range; in the case of mid-IR, one can mention ZnSe, $CaF_2$, $MgF_2$, and KBr as being among the most popular optical materials. In our study, we take ZnSe as a model system due to its relatively large bandgap, well-studied linear- and nonlinear optical properties,[15,18] and low absorption in both near-IR and mid-IR spectral ranges. The sketch of the experimental setup is shown in Fig. 1(a). Tunable-frequency mid-IR pulses are generated by an optical parametric amplifier (OPA; *Light Conversion* Orpheus-HE) pumped by a femtosecond laser system (*Light Conversion* Pharos) producing a train of pulses with a repetition rate of 3 kHz; central wavelength $\lambda_0 = 1028$ nm; pulse duration of $\tau_{FWHM} = 270$ fs and 2 mJ/pulse. A small fraction (5%) of the main beam from the amplifier is split off and used as a near-IR probe, while the main part pumps the OPA to produce $\lambda = 4.5\ \mu$m pulses used as a mid-IR pump. Pump and probe pulses are spatially and temporally overlapped inside a $d = 1.25$ mm-thick, polycrystalline ZnSe sample (*Crystran Ltd*). After the sample, the XPM-affected probe beam is spectrally analyzed with a monochromator (*Horiba* H10) connected to an avalanche photo-diode (*Becker-Hickl* APM-400-P-078). To increase the signal-to-noise ratio, the signal from the detector is first passed through a boxcar integrator (*SRS* SR250) before being analyzed in a lock-in amplifier (*SRS* SR830).

In the experiment, we record the spectrum of the probe beam at the exit from the sample for every value of pump-probe delay as shown in Fig. 1(c). In the range where pump and probe overlap temporally, the spectrum of the probe is visibly perturbed by the pump. As can be seen in Figs. 1(c) and Fig. 2, the spectral shift is changing sign depending on time delay between pump and probe pulses. Qualitatively, the character of the spectral change is in line with what one expects from XPM, which can be intuitively understood as shown in Fig. 1(b). As a result of Kerr effect, the refractive index $n_0$ of a medium acquires a nonlinear correction $\delta n$ proportional to the intensity $I$ of the pump: $\delta n = n_2 I$, where $n_2$ is the nonlinear (Kerr) refractive index. Now, on the one hand, the total refractive index $n = n_0 + \delta n$ determines the total optical phase accumulated by the probe pulse with wavelength $\lambda = 2\pi c/\omega$ as it propagates through the sample of thickness $L$: $\phi = 2\pi n L/\lambda$. On the other, time derivative of the phase determines the probe frequency $\omega = \dot{\phi}$. It is then clear that since time-dependent pump intensity $I(t)$ modifies $\phi(t)$, the frequency $\delta\omega$ acquires a correction proportional to the following derivative:

$$\delta\omega = 2\pi \frac{L}{\lambda} n_2 \frac{dI(t)}{dt}.$$

Therefore, analyzing the value of XPM-induced spectral shift and knowing the properties of the pump pulse, such as its duration and peak intensity, one can, in principle, expect to be able to extract the value for nonlinear Kerr index $n_2$ of the medium.

Needless to say, this simple analysis is only valid for the artificial case of a monochromatic probe and a steadily growing pump intensity $I(t)$. In the more realistic case of pulsed pump and probe, a more

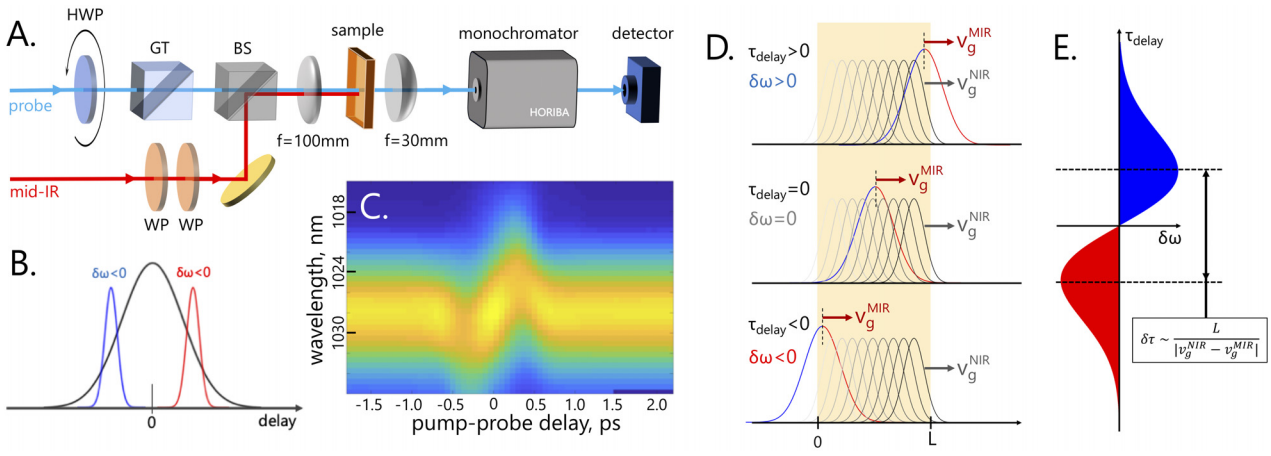


**FIG. 1.** (a) The setup to investigate XPM-induced spectral shift. Intensity of the probe is controlled via a half-wave plate (HWP) and Glan–Taylor polarizer (GT); the intensity of the mid-IR pump coming from an OPA is tuned by a pair of wire-grid polarizers (WP). Pump and probe beams are joined by a beam splitter (BS) and focused onto the sample with f = 100 mm lens. After the sample, the probe beam is re-collimated with f = 30 mm lens and after passing through monochromator detected by an avalanche photodiode detector. (b) A cartoon demonstrating cross-phase modulation (XPM) in the ideal case of no walk-off between pulses. The probe beam frequency is red- or blue-shifted depending on the sign of the Kerr index and instantaneous time derivative of pump intensity (black) (difference in pump- and probe pulse durations is exaggerated for the purpose of illustration). (c) Experimental XPM-induced spectral shift of a $\lambda_0 = 1028$ nm probe by a $\lambda_{pump} = 4500$ nm pump in a polycrystalline ZnSe sample as a function of pump-probe delay at peak pump intensity $I_0 = 2.2 \times 10^{14}$ W/cm$^2$. (d) XPM with non-matching pump and probe pulse group velocities $v_g^{MIR}$ and $v_g^{NIR}$, respectively ($v_g^{MIR} < v_g^{NIR}$). (e) XPM-induced spectral changes for the situation laid out in (d). Evidently, in the limit of large group velocity mismatch $\Delta v_g$, the temporal separation between extremal shifts (blue and red) is determined by $\Delta v_g$ rather than original pump pulse width.

20 September 2023 11:35:16


© Author(s) 2023

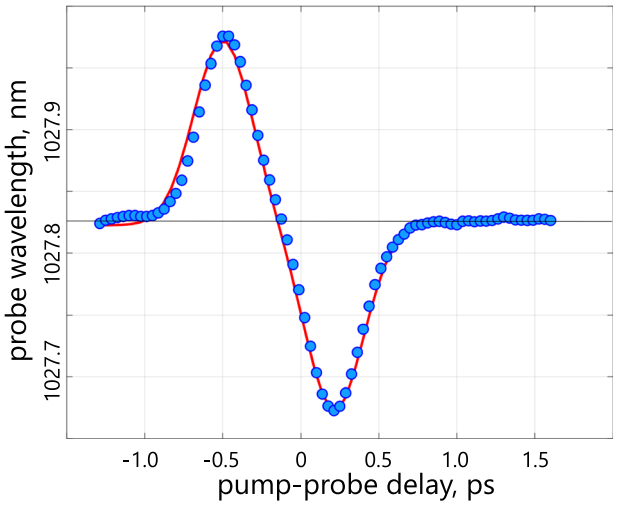


**FIG. 2.** Blue dots: XPM-induced spectral shift of the central wavelength of the probe pulse as a function of pump-probe delay at a peak pump intensity $I_0 = 2.1 \times 10^{13}$ W/cm$^2$; solid red curve: the result of the corresponding CGNLSE simulation.

involved analysis is necessary. The most important issue in a real experiment is that unlike the situation depicted in Fig. 1(b), the duration of pump and probe pulses are similar, which means that different parts of the latter experience different spectral shifts. Another problem can be seen upon inspecting Fig. 1(c) or Fig. 2. Here, one can see that the points of maximum spectral shifts are separated by about $\delta\tau \approx 0.7$ ps. This is considerably more than the pulse width of both the pump and probe pulses ($\tau_{pr} \approx \tau_{pu} \approx 270$ fs), which according to the naive cartoon in Fig. 1(b) should set the value for $\delta\tau$. This discrepancy comes from the fact that due to large wavelength difference, the mid-IR pump and near-IR probe pulses propagate through the sample with significantly different group velocities. Then, the interaction between the pulses occurs more like Fig. 1(d) ($v_g^{NIR} > v_g^{MIR}$). Here, in the generic situation when the two pulses meet in the middle of a sufficiently thick sample, each temporal segment of the probe (gray) experiences the entire pump (red-blue) pulse; therefore, a net spectral shift in the former integrates to zero. The spectral shift becomes non-zero only when the delay between the pulses is such that they overlap near one of the sample edges. The maximum spectral shifts then are achieved when the probe pulse center coincides with one of the slopes of the pump pulse. The separation between these points is consequently $\delta\tau \approx L/|v_g^{NIR} - v_g^{MIR}|$ (for $\delta\tau \gg \tau_{pu}$).

To accurately take these effects into account, we simulate the interaction between pulses by means of solving a system of coupled generalized nonlinear Schroedinger equations (CGNLSE) for frequency-nondegenerate fields[19] (see the supplementary material for details). In order to simplify the calculation, we ignore all absorption effects, which is justified since $\hbar(\omega + \Omega) < \Delta_{gap}$, where $\Delta_{gap}$ is the bandgap of ZnSe and $\omega$ and $\Omega$ are probe and pump frequencies, respectively.

In Fig. 2, we plot the central wavelength of the probe as a function of delay between the pump and probe pulses (blue dots) taken with a peak pump pulse intensity of $I_0 = 2.1 \times 10^{13}$ W/cm$^2$. This relatively moderate value was chosen to avoid various heating- and multi-photon-absorption-related phenomena not accounted for in our calculation. The solid red line in Fig. 2 is the result of a CGNLSE simulation with $n_2 \approx 0.65 \times 10^{-18}$ m$^2$/W. Given the excellent agreement, we take it as the measured value for the non-degenerate nonlinear Kerr index of (polycrystalline) ZnSe.

In the last step, we need to relate the value for the non-degenerate mid-IR/near-IR Kerr index $n_2(\omega, \Omega)$ to the degenerate mid-IR value $n_2(\Omega, \Omega)$. To this end, we note that generally speaking, in the limit $\omega^2, \Omega^2 \ll \Delta_{gap}^2$ Kerr index must have the following form:

$$n_2(\omega, \Omega) \propto 1 + \Gamma \times \left( \frac{\omega^2 + \Omega^2}{\Delta_{gap}^2} \right) \quad (1)$$

with $\Gamma$ being some numeric factor on the order of unity whose exact value depends on the microscopic details of a given material. The form of Eq. (1) is dictated by the fact that on the one hand, $n_2(\omega, \Omega)$—being an observable quantity—must be an even function of both $\omega$ and $\Omega$, and on the other hand, it must be symmetric against $\omega \leftrightarrow \Omega$ owing to Kleinman symmetry, which holds in the low-frequency limit.[20] Having said that $\Gamma$ is not expected to differ significantly from unity, we can also calculate its value for the specific case of two-band model,[21] which is known to adequately capture nonlinear properties of ZnSe.[17] Fitting the expression for $n_2(\omega, \Omega)$ (see the supplementary material) around the origin with Eq. (1) gives $\Gamma = 1.35$. The accuracy of the low-frequency expansion in Eq. (1) can be seen in Fig. 3, where we plot $n_2(\omega, \Omega)$, as calculated according to the two band model, and mark the experimental conditions of the present work with a red spot. As seen, the quadratic approximation provides a satisfactory agreement in a broad region around the origin which includes the wavelengths used in the present work. Using Eq. (1) and the value for non-degenerate $n_2$, we obtain a value for degenerate nonlinear Kerr

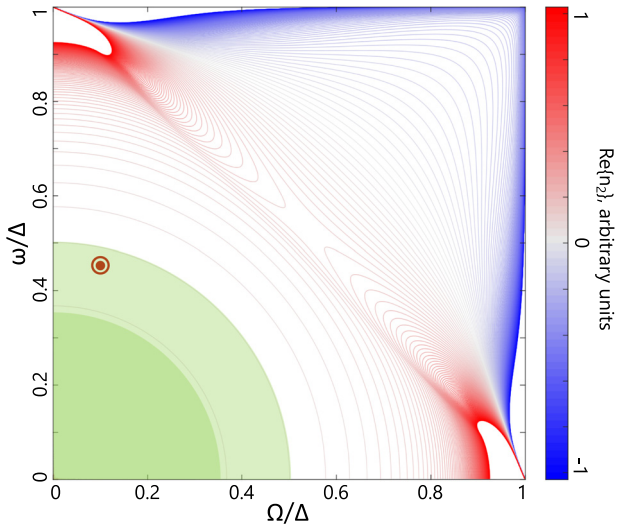


**FIG. 3.** Real part of nondegenerate Kerr index $n_2(\omega, \Omega)$ calculated for two-band model through dispersive analysis of Sheik-Bahae *et al.* In the shaded regions, the relative error of the approximate expression in Eq. (1) does not exceed 2% (darker green) and 10% (light green). The red spot marks the point that corresponds to the conditions of the present experiment ($\omega/\Delta \approx 0.45$, $\Omega/\Delta \approx 0.10$ with $\Delta = 2.82$ eV for ZnSe).

20 September 2023 11:35:16


© Author(s) 2023

index of polycrystalline ZnSe $n_2^{poly} \approx (0.5 \pm 0.1) \times 10^{-18}$ m$^2$/W at $\lambda = 4.5\ \mu$m; the main source of error here comes from the determination of the pump beam intensity (see the supplementary material). This number is similar in magnitude, albeit slightly less than the values obtained previously for single-[15] and poly-crystalline ZnSe samples.[13,14,22]

Finally, one might be interested in the dependence of the magnitude of cross-phase modulation on the polarizations of pump and probe beams. The brute force approach would be to redo the spectral analysis above for all possible polarization configurations. Such an experiment is certainly doable, albeit time consuming. However, as we show below, it is in fact not necessary when one is not after absolute values for susceptibilities but is only interested in the ratios between the different components of the nonlinear susceptibility tensor $\chi^{(3)}_{\alpha\beta\gamma\delta}$. Since XPM was established above as the main interaction channel between pump and probe pulses, one can take it for granted. Then, we note that the wavelength of the probe $\lambda = 1028$ nm lies in the range where the sensitivity of a Si photodiode-based detector has a strong wavelength dependence [see inset in Fig. 4(a) for the responsivity of a *Thorlabs* PDA100A2 detector used here]. Therefore, any pump-induced changes in the probe spectrum will be detected by it.

In Fig. 4(a), we show the transient signal at 1028 nm obtained in the standard transmission-geometry pump-probe configuration with collinear pulses having collinear polarizations (see the supplementary material for details). As expected for XPM, the transient has a bi-polar character, qualitatively similar to Fig. 2. The peak-to-peak amplitude of the signal $A_{pp}$ in Fig. 4(a) can, therefore, be used as a measure of XPM, and consequently Kerr index $n_2$. In Fig. 4(b), we plot this quantity as a function of the angle $\theta$ between pump and probe polarizations (blue dots). This simple angular dependence of the Kerr index $n_2(\theta)$ in a polycrystalline sample is natural and can be used to find relations between the various components of the susceptibility tensor. Indeed, when expressed in terms of crystalline nonlinear susceptibility $\chi_{\alpha\beta\gamma\delta}$, the effective nonlinear susceptibility of a polycrystalline sample $\chi_{\text{eff}}(\theta)$ must have the following form (see the supplementary material):

$$n_2(\theta) \propto \chi_{\text{eff}}(\theta) = \frac{1}{2}(\chi_{xxxx} + \chi_{xxyy}) + \frac{\cos(2\theta)}{4}(\chi_{xxxx} - \chi_{xxyy} + \chi_{xyyx} + \chi_{xyxy}). \quad (2)$$

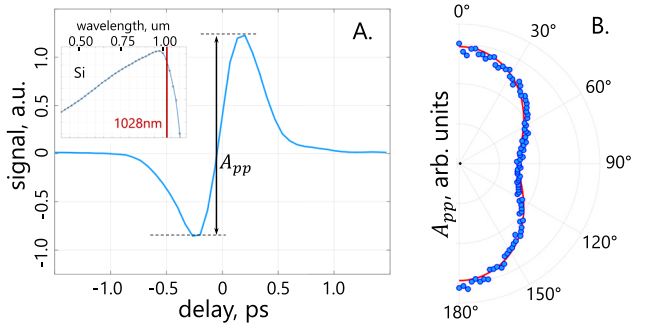


**FIG. 4.** (a) Signal at the Si-diode photodetector detecting probe beam after it was modified by the pump through XPM for collinear polarization orientation of pump and probe beams. Inset: sensitivity of the Si-based photodiode used in this work as a function of wavelength;[23] the red vertical line shows the probe beam wavelength; (b) Blue dots: peak-to-peak ($A_{pp}$) amplitude of the signal at the detector as a function of angle $\theta$ between pump and probe polarizations; red line: fit to $a + b\cos(2\theta)$.

The red solid curve in Fig. 4(b) is a fit $\chi_{\text{eff}}(\theta) = a + b\cos(2\theta)$ producing an experimental value for $b/a \approx 1/3$ that can be used to obtain the ratio between the quantities in the parentheses. For this, we note that for a cubic crystal structure of ZnSe $\chi_{xxxx} \approx \chi_{xxyy} + \chi_{xyyx} + \chi_{xyxy}$,[24] and find that for ZnSe at 4.5 $\mu$m pump and 1.03 $\mu$m probe, $\chi_{xxyy} \approx \chi_{xxxx}/2$ and $\chi_{xyxy} = \chi_{xyyx} \approx \chi_{xxxx}/4$.

In conclusion, we introduced an alternative technique to measure the nonlinear Kerr index in the mid-infrared range by studying the effects of cross-phase modulation on a secondary near-infrared probe beam. Employing this near-IR beam as a probe allowed circumventing the necessity for sophisticated IR detectors necessary for conventional methods such as z-scan. In order to relate the measured non-degenerate and the sought-after degenerate mid-IR Kerr indices, we analyzed the frequency dependence of nonlinear refractive index and with the help of nonlinear dispersive analysis of Sheik-Bahae *et al.*, we established a general expression for the frequency dependence of non-degenerate $n_2(\omega, \Omega)$ that was not limited to a specific material. In the proof-of-principle experiment, we measured the Kerr index for a poly-crystalline ZnSe sample to find $n_2 \approx (0.5 \pm 0.1) \times 10^{-18}$ m$^2$/W at 4.5 $\mu$m.

See the supplementary material for the supporting content.

The work was supported by IST Austria. The authors would like to gratefully acknowledge the help and assistance of Professor John M. Dudley.

## AUTHOR DECLARATIONS

### Conflict of Interest

The authors have no conflicts to disclose.

### Author Contributions

**Dusan Lorenc:** Conceptualization (equal); Formal analysis (equal); Methodology (equal); Writing – original draft (equal). **Zhanybek Alpichshev:** Conceptualization (equal); Formal analysis (equal); Investigation (equal); Methodology (equal); Supervision (equal); Writing – original draft (equal).

## DATA AVAILABILITY

The data that support the findings of this study are available from the corresponding author upon reasonable request.

## REFERENCES

[1]N. Bloembergen, R. K. Chang, S. S. Jha, and C. H. Lee, "Optical second-harmonic generation in reflection from media with inversion symmetry," Phys. Rev. **174**, 813–822 (1968).
[2]G. Cerullo and S. D. Silvestri, "Ultrafast optical parametric amplifiers," Rev. Sci. Instrum. **74**, 1–18 (2003).
[3]J. Li, J. Lu, A. Chew, S. Han, J. Li, Y. Wu, H. Wang, S. Ghimire, and Z. Chang, "Attosecond science based on high harmonic generation from gases and solids," Nat. Commun. **11**, 2748 (2020).
[4]M.-C. Chen, C. Mancuso, C. Hernández-García, F. Dollar, B. Galloway, D. Popmintchev, P.-C. Huang, B. Walker, L. Plaja, A. A. Jaroń-Becker, A. Becker, M. M. Murnane, H. C. Kapteyn, and T. Popmintchev, "Generation of bright isolated attosecond soft x-ray pulses driven by multicycle midinfrared lasers," Proc. Natl. Acad. Sci. U.S.A. **111**, E2361–E2367 (2014).

20 September 2023 11:35:16


© Author(s) 2023

[5]V. Y. Fedorov and S. Tzortzakis, "Powerful terahertz waves from long-wavelength infrared laser filaments," Light: Sci. Appl. **9**, 186 (2020).
[6]R. W. Boyd, *Nonlinear Optics*, 3rd ed. (Academic Press, Burlington, 2008).
[7]P. B. Chapple, J. Staromlynska, J. A. Hermann, T. J. Mckay, and R. G. Mcduff, "Single-beam z-scan: Measurement techniques and analysis," J. Nonlinear Opt. Phys. Mater. **06**, 251–293 (1997).
[8]B. Taheri, H. Liu, B. Jassemnejad, D. Appling, R. C. Powell, and J. J. Song, "Intensity scan and two photon absorption and nonlinear refraction of $C_{60}$ in toluene," Appl. Phys. Lett. **68**, 1317–1319 (1996).
[9]M. Samoc, A. Samoc, B. Luther-Davies, Z. Bao, L. Yu, B. Hsieh, and U. Scherf, "Femtosecond z-scan and degenerate four-wave mixing measurements of real and imaginary parts of the third-order nonlinearity of soluble conjugated polymers," J. Opt. Soc. Am. B **15**, 817 (1998).
[10]J. J. Pigeon, S. Y. Tochitsky, E. C. Welch, and C. Joshi, "Measurements of the nonlinear refractive index of air, $N_2$, and $O_2$ at 10 $\mu$m using four-wave mixing," Opt. Lett. **41**, 3924–3927 (2016).
[11]R. Adair, L. L. Chase, and S. A. Payne, "Nonlinear refractive index of optical crystals," Phys. Rev. B **39**, 3337–3350 (1989).
[12]I. Kang, T. Krauss, and F. Wise, "Sensitive measurement of nonlinear refraction and two-photon absorption by spectrally resolved two-beam coupling," Opt. Lett. **22**, 1077 (1997).
[13]G. Jansonas, R. Budriūnas, M. Vengris, and A. Varanavičius, "Interferometric measurements of nonlinear refractive index in the infrared spectral range," Opt. Express **30**, 30507 (2022).
[14]T. R. Ensley and N. K. Bambha, "Ultrafast nonlinear refraction measurements of infrared transmitting materials in the mid-wave infrared," Opt. Express **27**, 37940 (2019).
[15]G. N. Patwardhan, J. S. Ginsberg, C. Y. Chen, M. M. Jadidi, and A. L. Gaeta, "Nonlinear refractive index of solids in mid-infrared," Opt. Lett. **46**, 1824 (2021).
[16]M. Sheik-Bahae, J. Wang, and E. V. Stryland, "Nondegenerate optical Kerr effect in semiconductors," IEEE J. Quantum Electron. **30**, 249–255 (1994).
[17]D. C. Hutchings, M. Sheik-Bahae, D. J. Hagan, and E. W. V. Stryland, "Kramers-Krönig relations in nonlinear optics," Opt. Quantum Electron. **24**, 1–30 (1992).
[18]M. J. Weber, *Handbook of Optical Materials* (CRC Press, 2018).
[19]G. P. Agrawal, *Nonlinear Fiber Optics* (Elsevier, 2013).
[20]R. W. Boyd, "Order-of-magnitude estimates of the nonlinear optical susceptibility," J. Mod. Opt. **46**, 367–378 (1999).
[21]M. Sheik-Bahae, D. Hutchings, D. Hagan, and E. V. Stryland, "Dispersion of bound electron nonlinear refraction in solids," IEEE J. Quantum Electron. **27**, 1296–1309 (1991).
[22]K. Werner, M. G. Hastings, A. Schweinsberg, B. L. Wilmer, D. Austin, C. M. Wolfe, M. Kolesik, T. R. Ensley, L. Vanderhoef, A. Valenzuela, and E. Chowdhury, "Ultrafast mid-infrared high harmonic and supercontinuum generation with $N_2$ characterization in zinc selenide," Opt. Express **27**, 2867 (2019).
[23]PDA100A2 Detector Characteristics, Thorlabs, Inc.
[24]W. K. Burns and N. Bloembergen, "Third-harmonic generation in absorbing media of cubic or isotropic symmetry," Phys. Rev. B **4**, 3437–3450 (1971).

20 September 2023 11:35:16


© Author(s) 2023